Physics Letters B 755 (2016) 162–167

Contents lists available at ScienceDirect

Physics Letters B

www.elsevier.com/locate/physletb

Spectral caustics in laser assisted Breit–Wheeler process

T. Nousch [a,b,*], D. Seipt [c], B. Kämpfer [a,b], A. I. Titov [d]

[a] Helmholtz-Zentrum Dresden-Rossendorf, Institut für Strahlenphysik, PF 510119, D-01314 Dresden, Germany
[b] Institut für Theoretische Physik, TU Dresden, D-01062 Dresden, Germany
[c] Helmholtz-Institut Jena, Fröbelstieg 3, 07743 Jena, Germany
[d] Bogoliubov Laboratory for Theoretical Physics, Joint Institute for Nuclear Research, RU-141980 Dubna, Russia

ARTICLE INFO

Article history:
Received 8 September 2015
Received in revised form 22 January 2016
Accepted 29 January 2016
Available online 2 February 2016
Editor: A. Ringwald

Keywords:
Pair production
XFEL
Breit–Wheeler
Laser-assisted processes

ABSTRACT

Electron–positron pair production by the Breit–Wheeler process embedded in a strong laser pulse is analyzed. The transverse momentum spectrum displays prominent peaks which are interpreted as caustics, the positions of which are accessible by the stationary phases. Examples are given for the superposition of an XFEL beam with an optical high-intensity laser beam. Such a configuration is available, e.g., at LCLS at present and at European XFEL in near future. It requires a counter propagating probe photon beam with high energy which can be generated by synchronized inverse Compton backscattering.

1. Introduction

Pair production processes in electromagnetic interactions are of permanent interest due to fundamental aspects to be addressed up to technological relevance for material investigations. The basic process of two-photon conversion into a pair of electron (e^-) + positron (e^+), symbolically $X' + X \to e^+ + e^-$ as $2 \to 2$ reaction of photons with four-momenta $k_{X',X} \sim (\omega_{X',X}, \mathbf{k}_{X',X})$ has been evaluated by Breit and Wheeler [1] within a framework which is called nowadays perturbative quantum electro dynamics (pQED). It is a t-channel process in lowest order pQED. There are many other elementary processes with emerging pairs which are accessible theoretically by pQED, for instance such ones with $\mu^+ + \mu^-$ in the final state [2], or even with $\bar{\nu} + \nu$ [3].

Pair production is a threshold process, meaning that a certain minimum energy must be provided in the entrance channel to have $e^+ + e^-$ with energy $> 2m$ in the exit channel (m is the electron rest mass). This implies that the energies of the X' and X photons must be sufficiently large to overcome the threshold, i.e. $s_{X'X} = (k_{X'} + k_X)^2 = 2\omega_{X'}\omega_X(1 - \cos\theta_{X'X}) > 4m^2 \equiv s_{\rm thr}$, where the relative angle $\theta_{X'X}$ of both beams is π for head-on collisions. In the considered $2 \to 2$ scattering process, $s_{X'X}$ equals the invariant mass of the produced electron–positron pair.

In case the initial center-of-mass energy is below the production threshold of the $2 \to 2$ process, $s_{X'X} < s_{\rm thr}$, pairs can still be produced via multi-photon effects. This particularly interesting process has been investigated in the SLAC experiment E-144 [4,5], where a high-energy photon (several GeV) was colliding with an intense optical laser pulse (L). While the $2 \to 2$ reaction was kinematically forbidden, the multi-photon channels $X + nL \to e^+ + e^-$ with $n > 1$ had sufficient center-of-mass energy $s_{X,nL} = (k_X + nk_L)^2$ to overcome the pair production threshold. This process is called laser-induced multi-photon Breit–Wheeler pair production. In fact the high-energy photon was produced via Compton backscattering of laser light on 46.6 GeV electrons in the same laser focal spot. (For a recent theoretical re-analysis see e.g. Ref. [6].) The multi-photon channels only have a considerable probability if the laser pulse is sufficiently intense.

The laser intensity parameter $a_0 = |e|E_L/m\omega_L$ (with $-|e|$ as the electron charge, and E_L and ω_L refer to the field strength and frequency of the laser) delineates the non-relativistic domain, $a_0 < 1$, and the relativistic domain, where $a_0 > 1$ [7]. Moreover, a_0 quantifies the relevance of multi-photon effects; it is the inverse Keldysh adiabaticity parameter of the process. Another important parameter that classifies the pair production is the non-linear quantum parameter $\chi_\gamma = \frac{1}{2}a_0 s_{X,1L}/s_{\rm thr}$ that combines a_0 and the kinematics of the process. For $a_0 \lesssim 1$ and $\chi_\gamma \lesssim 1$ only a few multi-photon channels contribute, and the probability for the nth (open) channel behaves roughly as $W_n \sim a_0^{2n}$. For $a_0 \gg 1$ and $\chi_\gamma \lesssim 1$ (i.e. the $2 \to 2$ process is extremely deep below the threshold and huge

* Corresponding author.
E-mail addresses: t.nousch@hzdr.de (T. Nousch), d.seipt@gsi.de (D. Seipt).

http://dx.doi.org/10.1016/j.physletb.2016.01.062

amounts of laser photons are required) the probability behaves semi-classically [8]. The formation region of the pair becomes much shorter than the laser cycle, $\propto 1/a_0$, and the process takes place instantaneously as it were in a local constant crossed field. For $\chi_\gamma \ll 1$ the Breit–Wheeler pair production probability is exponentially suppressed in the semi-classical regime, $W \sim e^{-8/3\chi_\gamma}$ [9], with the same functional dependence on the electric field strength as Schwinger pair production [10–14]. (For Schwinger pair production, the impact of an assisting high-frequency field has been studied, e.g. in [15–17].)

The laser-induced multi-photon Breit–Wheeler process has been investigated exhaustively (see e.g. Refs. [9,10,18]) for long-duration pulses of the laser beam. The process becomes markedly modified for ultra-short laser pulses: The temporal pulse structure, even in the plane-wave limit, gives a dominating impact specific for the pulse shape [19–24]. In a finite pulse of the laser beam there are several interfering effects: finite bandwidth (i.e. ω_L is the central frequency and higher and lower frequencies contribute to the power spectrum), multi-photon effects (i.e. the above mentioned higher harmonics) and the intensity-dependent threshold shifts [25,26].

Due to the small frequency of optical lasers, $\omega_L = \mathcal{O}(1\text{ eV})$, the parameter χ_γ is very small unless the frequency of the colliding photon X is very high – on the order of several GeV. This makes the non-linear Breit–Wheeler pair production exceedingly small in pure optical laser–laser collisions unless both lasers have ultra-high intensities (of the order of the Sauter Schwinger field 4×10^{29} W/cm^2) [10–12,18]. With the advent of X-ray free electron lasers (XFELs) that can provide photons with $\omega_X = \mathcal{O}(10\text{ keV})$ at high intensities, the gap to the threshold is diminished, but still fairly large, unless $\omega_{X'} = \mathcal{O}(50\text{ MeV})$. Therefore, one can ask whether the assistance of an ultra-high intensity laser beam L enables pair production if $s_{X'X}$ is in the sub-threshold region. Clearly, also here, very strong non-linear effects due to an ultra-high intensity laser beam are required for enabling this *laser-assisted Breit–Wheeler pair production*. A related issue is the modification of the Breit–Wheeler process by an assisting laser beam above the threshold.

To attempt a description of this latter process, we consider here the reaction $X' + (X + L) \to e^+ + e^-$, that is the laser assisted linear Breit–Wheeler process, where $s_{X'X} > s_{\rm thr}$ and X is a weak field in the sense of $a_X \ll 1$ for the above defined intensity parameter a_0 transferred here to the other individual fields; the probe photon field is anyhow considered as weak, $a_{X'} \ll 1$, i.e. only one photon from the field X' participates in a single pair production event. We have in mind the combination of an XFEL beam X with a synchronized, co-propagating laser beam L which may be strong. To be specific, the intensity parameter of X is less than $a_X = \mathcal{O}(10^{-2})$ according to [27], and for the L beam from a PW-class laser we let be $a_L = \mathcal{O}(1)$. Note that $a_{X,L}$ depend on the size of the actual focal spots. Our considerations below apply to the homogeneity region where a plane-wave approximation holds, but we include for the first time the temporal pulse shapes as an essential element in combination with the large frequency ratio $\omega_X/\omega_L \equiv \eta^{-1} \gg 1$. Considering the European XFEL beam, under construction (and near to completion) in Hamburg/DESY [28], in the HIBEF project [29] with $\omega_X = 6$ keV, the counter-propagating beam X' must have about $\omega_{X'} = 60$ MeV F (accessible, for instance, by suitable inverse Compton back-scattering of laser light off laser-accelerated electrons [30–35]) to allow for the linear Breit–Wheeler process. In the equal-momentum frame, $\mathbf{k}_{X'} = -\mathbf{k}_X$, we have $\omega_{X'} = \omega_X = 600$ keV as geometric mean of the laboratory frequencies and $s_{X'X}/s_{\rm thr} = 1.38$. For the assisting laser field we assume an UV laser frequency of 10 eV in the laboratory frame, i.e. $\omega_L = 1$ keV in the equal-momentum frame. In this set-up, the pairs cannot be produced by the $X' - L$ collisions alone: This process is extremely below the threshold and, thus, extremely suppressed since $s_{X'L}/s_{\rm thr} = 0.002$ and $\chi_\gamma = 0.001 a_L$.

Our analysis in some aspects parallels [36,37], where the laser assisted Compton process is analyzed. This cross channel enjoys some remarkable features: The spectrum of Compton scattered X-ray photons off an electron moving in an accelerated manner in an external laser pulse displays, besides the well-known Compton line at fixed observation angle, a number of prominent peaks, and the complicated spectral distribution exhibits distinct regions with changing patterns. The striking finding in [37] is the interpretation of the prominent peaks as spectral caustics related to merging stationary phase points. Accounting for quantum interference effects for the emission from different locations of the quasi-classical electron motion in the laser field along a temporally changing figure-8 trajectory, the gross features of the complicated spectrum become easily accessibly. Such an interpretation is also in the spirit of [8], where the spectrum of pairs produced in a strong external field[1] is explained as redistribution in phase space following the production process (which can be approximated by a temporally constant cross-field probability) and keeping interference effects.

Despite of the similarities of the Compton and Breit–Wheeler processes related by crossing symmetry, the different phase spaces and attributed kinematic relations make them fairly different. In addition, the Compton process has a classical limit – the Thomson scattering – while the pair-production is of genuine quantum nature. This is the reason for considering separately the analog of the spectral caustics in [37] in the laser assisted Breit–Wheeler process.

Our paper is organized as follows. In section 2 we present the QED basics for the calculation of the laser assisted Breit–Wheeler process. Selected numerical results are discussed in section 3 for a special kinematic situation to highlight the impact of the laser field. Section 4 summarizes.

2. The QED process

In the Furry picture, the process $X' + (X + L) \to e^+ + e^-$ is described by a one-vertex diagram $X' \to e^+_{X+L} + e^-_{X+L}$ (see Fig. 1, left), where $e^\pm_{X+L}$ mean the Volkov solutions of out-going electrons and positrons in temporally shaped fields $X + L$, both ones co-propagating and with perpendicularly linear polarization. We consider head-on collision of the photons X' and $X + L$. These assumptions are made for the sake of simplifications of the subsequent evaluations. In addition, we linearize in the XFEL field A_X. This corresponds then to a Furry-picture two-vertex t-channel diagram (see Fig. 1, right), with exchange diagram analog to the Breit–Wheeler process $X' + X \to e^+_L + e^-_L$, where however here the out-going electron and positron and the propagator are laser dressed.

2.1. Kinematics

The energy–momentum balance for laser-assisted pair production can be put into the form (μ is a Lorentz index)

$$k^\mu_{X'} + k^\mu_X + \ell k^\mu_L = p^\mu_p + p^\mu_e\,, \tag{1}$$

where ℓ represents a hitherto unspecified momentum exchange parameter between the assisting laser field L and the produced pair (hereafter labeled by e and p for electron and positron, respectively). We define light-front coordinates, e.g. $x^\pm = x^0 \pm x^3$ and

[1] The interested reader is referred to [38–45] for further work on pair production in external fields within a QED framework.

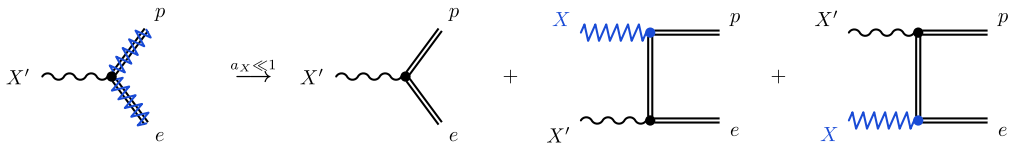

Fig. 1. Pair creation in the laser assisted Breit–Wheeler process (left diagram; the wavy line stands for the incoming probe photon X' and the double lines with superimposed zigzag are for outgoing laser + XFEL field dressed electron and positron). For weak XFEL fields, the leading order expansion results in the right diagrams where the double lines mean laser dressed wave functions and propagator and the zigzag line is for the XFEL X. The zeroth order process (in the field X) is just the laser-induced Breit–Wheeler pair-production in $L - X'$ collisions studied extensively in the literature. For our considered parameters this channel is strongly suppressed and will not be considered further.

$\mathbf{x}_\perp = (x^1, x^2)$ and analogously the light-front components of four-momenta. They become handy because the laser four-momentum vectors only have one non-vanishing light-front component $k^-_{L,X} = 2\omega_{L,X}$. In particular, Eq. (1) contains the three conservation equations in light-front coordinates: $k^+_{X'} = p^+_p + p^+_e$ and $\mathbf{p}^\perp_e = -\mathbf{p}^\perp_p$. Moreover, the knowledge of all particle momenta allows to calculate ℓ via the fourth equation of (1)

$$\ell = \frac{1}{\eta}\left(\frac{p^-_p + p^-_e - k^-_{X'}}{k^-_X} - 1\right), \tag{2}$$

with the frequency ratio $\eta = \omega_L/\omega_X \ll 1$. (Note that the variable ℓ can be related also to $M^2 = (1+\eta\ell)s_{X'X}$, where M is the invariant e^+e^- mass.) It is convenient to parametrize the produced positron's phase space by the following three variables: (i) the momentum exchange parameter ℓ, (ii) the azimuthal angle φ with respect to the polarization direction of the assisting laser field and (iii) the shifted rapidity

$$z = \frac{1}{2}\ln\left(\frac{p^+_p}{p^-_p}\right) + \frac{1}{2}\ln\left(\frac{(1+\eta\ell)\,\omega_X}{\omega_{X'}}\right). \tag{3}$$

The case $z = 0$ distinguishes the *symmetric* situation where the longitudinal laser momentum is equally shared between the electron and the positron. In particular, in the equal-momentum frame each particle acquires the longitudinal momentum $p_\parallel = (p^+ - p^-)/2$ Treating (ℓ, z, φ) as independent variables completely specifies the four-momentum p_p of the produced positron by using Eq. (3) and

$$p^2_{\perp p} = m^2\left(\frac{1+\eta\ell}{\cosh^2 z}\frac{s_{X'X}}{s_{\text{thr}}} - 1\right). \tag{4}$$

Moreover, Eq. (1) allows to eliminate the dependence on the produced electron's momentum p_e.

The laser pulses $X + L$ are described by the four-vector potential

$$A^\mu = \frac{m a_L}{e} g_L(\eta\phi)\,\epsilon^\mu_L \cos(\eta\phi) + \frac{m a_X}{e} g_X(\phi)\,\epsilon^\mu_X \cos\phi \tag{5}$$

with the transverse polarization four-vectors $\epsilon^\mu_{L,X}$ obeying $k_{L,X}\cdot\epsilon_{L,X} = 0$ (a dot indicates the scalar product of four-vectors) and $\epsilon_X \cdot \epsilon_L = 0$, and the pulse envelope functions

$$g_L(\phi) = \begin{cases} \cos^2\left(\frac{\pi\phi}{2\tau_L}\right) & , -\tau_L \le \phi \le \tau_L\,, \\ 0 & , \text{otherwise}\,, \end{cases} \tag{6}$$

$$g_X(\phi) = \exp\left(\frac{-\phi^2}{2\tau^2_X}\right) \tag{7}$$

with the dimensionless pulse lengths parameters $\tau_{L,X}$. The invariant phase is defined as $\phi = k_X \cdot x = \omega_X x^+$.

2.2. Matrix element and cross section

The invariant matrix element for the process depicted in the left diagram of Fig. 1 reads

$$\mathcal{S} = -ie\int dx\,\bar\Psi_{X+L}\not\epsilon_{X'} e^{ik_{X'}\cdot x}\Psi_{X+L}\ , \tag{8}$$

where $\not\epsilon_{X'}$ is the four-polarization vector of the probe photon X' contracted with a Dirac matrix (we use Feynman's slash notation) and $\bar\Psi_{X+L}$ stands for the Volkov solution of the outgoing electron

$$\bar\Psi_{X+L} = \bar u(p_e)\left(1 + \frac{e\not k_X \not A}{2k_X\cdot p_e}\right)e^{-iS_{pe}} \tag{9}$$

i.e. dressing by the field (5), and analogously for the out going positron

$$\Psi_{X+L} = \left(1 - \frac{e\not k_X \not A}{2k_X\cdot p_p}\right)e^{iS_{-pp}}\,v(p_p) \tag{10}$$

with the phase function

$$S_p = -p\cdot x - \int_{\phi_0}^{\phi} d\phi'\left(\frac{2eA(\phi)\cdot p - e^2A^2(\phi)}{2k_X\cdot p}\right); \tag{11}$$

u, v are free-field Dirac spinors, and $\bar u$, $\bar v$ their adjoints. ϕ_0 is an irrelevant constant of integration. The phase functions S_p are known [46] to coincide with the classical Hamilton–Jacobi actions for charged particles in a plane wave. Here, they appear via exact solutions of the Dirac equation and its adjoints in the field (5). These expressions still contain all orders in the X-ray field a_X. Since we assume a weak field we can linearize all expressions in a_X. For technical details of this linearization we refer the interested reader to Ref. [36]. By employing light-front coordinates we can perform three of the spatial integrals in (8), and represent the $\mathcal{S}$ matrix as $\mathcal{S} = 4\pi^3\, ie/\omega_{X'}\delta^2(\mathbf{p}^\perp_p + \mathbf{p}^\perp_e + \mathbf{k}^\perp_{X'})\delta(p^+_p + p^+_e + k^+_{X'})\mathcal{M}$ with the scattering amplitude $\mathcal{M}$ which is specified below in Section 2.3.

With help of this scattering amplitude we can write the positron's triple-differential cross section in laser-assisted Breit–Wheeler positron production as

$$\frac{d^3\sigma}{dz\,d\ell\,d\varphi} = \frac{\eta r_0^2 k^0_X}{4\pi\, p^+_e a^2_X \int_{-\infty}^{+\infty} d\phi\, g^2_X(\phi)} \times \frac{1-\tanh z}{\cosh^2 z}\,\frac{1}{2}\sum|\mathcal{M}|^2\,, \tag{12}$$

where we normalize by the particle density of the field X, $\rho_X = m^2 a^2_X/(2e^2)\int_{-\infty}^{\infty} d\phi g^2_X(\phi)$, and by the incoming photon flux $j_{in} = k_X\cdot k_{X'}/(k^0_X k^0_{X'}) = 2$. In this way, the cross section (12) turns into the usual Breit–Wheeler cross section for a vanishing assisting laser field. The sum runs over the unobserved spin degrees of freedom of the produced pair as well as the polarization states of the incident photon X'. Furthermore, we utilize the classical electron radius $r_0 = \alpha_{\text{QED}}/m$, with the fine structure constant $\alpha_{\text{QED}} \simeq 1/137$.

2.3. Linearized matrix element

Here we provide the explicit expression for the linearized scattering amplitude $\mathcal{M}$ for $a_X \ll 1$. As we argued above the zeroth-order term $\mathcal{O}(a_X^0)$ does not contribute to the pair production for our considered parameters. The leading term is $\mathcal{O}(a_X)$ and reads

$$\mathcal{M} = a_X(\mathcal{J}_X\mathcal{A}_0 - \alpha_X \sum_{k=0,1,2} \mathcal{J}_k\mathcal{A}_k)\,, \tag{13}$$

$$\alpha_X = \frac{1}{2}m\left(\frac{p_e\cdot\epsilon_X}{k_X\cdot p_e} - \frac{p_p\cdot\epsilon_X}{k_X\cdot p_p}\right). \tag{14}$$

Since $\mathcal{M}\propto a_X$ the $1/a_X^2$ in (12) cancels and the pair production cross section is independent of the intensity of the incident X-rays. The spin and polarization dependence is encoded in the transition operators with Dirac current structures

$$\mathcal{J}_0 = \bar{u}(p_e)\not{\epsilon}_{X'}v(p_p), \tag{15}$$

$$\mathcal{J}_1 = \frac{ma_L}{2}\bar{u}(p_e)\left(\frac{\not{\epsilon}_L\not{k}_X\not{\epsilon}_{X'}}{k_X\cdot p_p} - \frac{\not{\epsilon}_{X'}\not{k}_X\not{\epsilon}_L}{k_X\cdot p_e}\right)v(p_p), \tag{16}$$

$$\mathcal{J}_2 = \frac{m^2a_L^2k_X\cdot\epsilon_{X'}}{2(k_X\cdot p_p)(k_X\cdot p_e)}\bar{u}(p_e)\not{k}_Xv(p_p), \tag{17}$$

$$\mathcal{J}_X = \frac{m}{2}\bar{u}(p_e)\left(\frac{\not{\epsilon}_X\not{k}_X\not{\epsilon}_{X'}}{k_X\cdot p_p} - \frac{\not{\epsilon}_{X'}\not{k}_X\not{\epsilon}_X}{k_X\cdot p_e}\right)v(p_p), \tag{18}$$

with the polarization four-vector $\epsilon_{X'}$ of probe photon fulfilling $k_{X'}\cdot\epsilon_{X'}=0$. Note that the $\mathcal{J}_k$ defined in Eqs. (15)–(18) are just complex numbers, albeit depending on momenta, polarizations and spins.

The dynamics of the laser-assisted pair production process is described by the integrals

$$\mathcal{A}_j = \int_{-\infty}^{+\infty} d\phi\,[\cos(\eta\phi)\,g_L(\eta\phi)]^j\,g_X(\phi)\,e^{iH} \tag{19}$$

for $j=0,1,2$ (on l.h.s. a label, while on r.h.s. a power), with the phase

$$H = \int_{\eta\phi_0}^{\eta\phi} d\phi'\left(\ell + \frac{\alpha}{\eta}g_L(\phi')\cos(\phi') + \frac{\beta}{\eta}g_L^2(\phi')\cos^2(\phi')\right) \tag{20}$$

using the abbreviations

$$\alpha = ma_L\left(\frac{p_e\cdot\epsilon_L}{k_X\cdot p_e} - \frac{p_p\cdot\epsilon_L}{k_X\cdot p_p}\right), \tag{21}$$

$$\beta = \frac{(ma_L)^2}{2}\left(\frac{1}{k_X\cdot p_e} + \frac{1}{k_X\cdot p_p}\right). \tag{22}$$

Note that the phase H, Eq. (20), can be rewritten in terms of the classical trajectory of the generated positron moving in the assisting laser field, projected onto the four-momentum vector $k_{X'}$ of the probe photon:

$$H = \int_{\eta\phi_0}^{\eta\phi} d\phi'\left((1+\eta\ell)\frac{k_{X'}\cdot\pi_p(\phi')}{\eta k_{X'}\cdot p_p} - \frac{1}{\eta}\right), \tag{23}$$

where

$$\pi_p^\mu(\phi) = p_p^\mu + eA_L^\mu(\phi) - \frac{eA_L(\phi)\cdot p_p}{k_L\cdot p_p}k_L^\mu - \frac{e^2A_L^2(\phi)}{2k_L\cdot p_p}k_L^\mu \tag{24}$$

is the four-momentum of the positron (with out state momentum p_p^μ) along the trajectory in the laser field A_L^μ (first term in (5)) as a first integral of the Lorentz equation [47]. This suggests the interpretation of the pair creation by a plain Breit–Wheeler process $X'+X\to e^+ + e^-$ as the production process with a subsequent redistribution of the positrons in phase space due to the action of the laser field. By integrating over ϕ in Eq. (19) one coherently adds the production amplitudes from all "instants" (expressed by the laser phase) which—after the redistribution due to the laser field—contribute to the yield of positrons at the chosen final phase-space point (ℓ, z, φ).

The stationary phase condition $dH/d\phi = 0$ reads, by means of (20),

$$0 = \ell + \frac{\alpha}{\eta}g_L(\phi)\cos(\phi) + \frac{\beta}{\eta}g_L^2(\phi)\cos^2(\phi), \tag{25}$$

representing an approximation w.r.t. the highly oscillating phase factor $\exp(iH)$ in (19). Note that the large frequency ratio $\omega_X/\omega_L = \eta^{-1}\gg 1$ is decisive for that. The stationarity condition (25) furnishes a relation between the instant ϕ the pair is produced and the momentum exchange ℓ. In order to solve (25) for $\ell(\phi)$ we first need to work out how the coefficients α and β depend on ℓ. Here and in the following we restrict our investigation to those positrons that are detected in the polarization direction of the assisting laser, characterized by $\varphi=\pi$. By eliminating the electron momentum p_e in Eqs. (21) and (22) with help of Eq. (1) and by rewriting the scalar products in terms of the independent variables (ℓ, z, φ) we find $\alpha = -2\beta\sqrt{(1+\eta\ell)/\beta - a_L^{-2}}$ and $\beta = a_L^2 s_{\rm thr}\cosh^2(z)/s_{X'X}$. Using these expressions in Eq. (25) we obtain a quadratic equation for $\ell(\phi)$, with the two apparent solutions[2]

$$\ell_\pm(\phi) = \frac{\beta}{\eta}g_L(\phi)\cos(\phi)\left[g_L(\phi)\cos(\phi) \pm 2\sqrt{\frac{1}{\beta} - \frac{1}{a_L^2}}\right]. \tag{26}$$

One has to check, however, for which values of ϕ the $\ell_\pm(\phi)$ represent true solutions of the initial Eq. (25). These solutions for $\ell_\pm(\phi)$, which follow from the stationary phase condition, determine the amount of laser momentum that is transferred to the positron after its production at the instant ϕ, and finally arriving at the phase-space point (ℓ, z, φ). That means, positrons at some fixed ℓ in phase space are produced only at a few certain instants.

3. Numerical results and interpretation as spectral caustics

In Figs. 2–4, blue spectra in upper panels, we show numerical examples of the triple-differential positron production cross section $d^3\sigma/d\ell dz d\varphi$ for $z=0$ and $\varphi=\pi$. The chosen $\sqrt{s_{X'X}} = 1.2$ MeV is clearly above the threshold, $s_{X'X}/s_{\rm thr} = 1.38$, and the Breit–Wheeler peak at $\ell=0$ corresponding to $p_\perp = \frac{1}{2}\sqrt{s_{X'X}-s_{\rm thr}}$ is visible as pronounced structure.[3] The very rich-structured blue spectra in the upper panels of Figs. 2–4 exhibit the plain QED results based on Eqs. (12)–(22). To expose the strength distribution in a spectrum we apply a smoothing procedure yielding the red

[2] Note that for laser-assisted Compton scattering of X-rays studied in [37], the stationary phase condition provides a *linear* equation for $\ell(\phi)$ with the single solution $\ell(\phi) = 1/\eta(k'\cdot p_0/(k'\cdot\pi_e(\phi)) - 1)$ with k' denoting the four-momentum of the scattered photon, $\pi_e(\phi)$ the kinetic four-momentum of an electron in the laser pulse, and p_0 is the four-momentum of the electron before the laser pulse arrives. It is the relativistic kinematics of the massive out-particle instead of the massless photon in the case of Compton scattering which gives rise to the double root which leads to Eq. (26).

[3] Since we consider here exclusively the positron out-states, the label "p" is dropped.

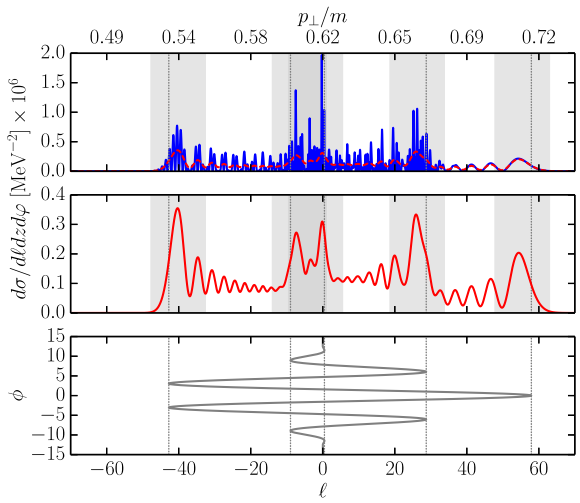

Fig. 2. Spectra for the laser assisted Breit–Wheeler process with the parameters mentioned in the Introduction which translate into $\sqrt{s_{X'X}} = 1.2$ MeV, $\eta = 1/600$, $a_X = 10^{-5}$, $\tau_X = 2\tau/(\pi\eta)$, $a_L = 0.1$, and $\tau_L = 4\pi$ in the field (2). Upper panel: $d\sigma/d\ell dz d\varphi$ at $z = 0$ and $\varphi = \pi$ as a function of ℓ (lower axis; the corresponding values of $p_\perp$ are given at the upper axis). The calculated spectrum according to (12) (blue, with 20,000 meshes) is smoothed by a Gaussian window function with width $\delta\ell = 0.8$ to get the red curve. Middle panel: smoothed spectrum separately. Lower panel: phase ϕ as a function of ℓ from Eq. (26) (only the "+" solution applies here). The vertical dotted lines depict the positions of diverging $d\phi/d\ell$, where two branches of $\phi(\ell)$ merge. The gray bands depict the estimated widths of caustic regions. (For interpretation of the references to color in this figure legend, the reader is referred to the web version of this article.)

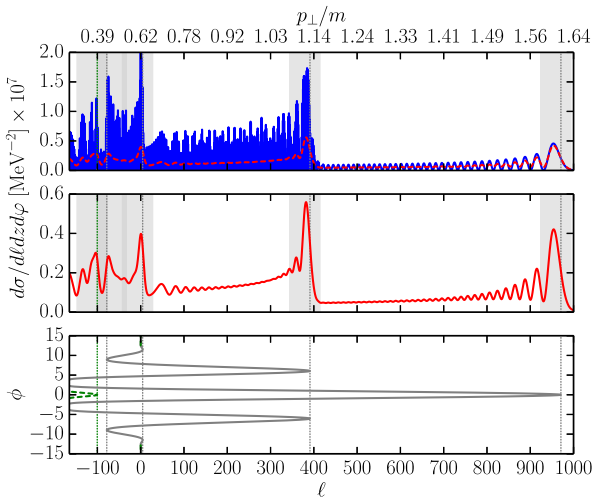

Fig. 3. As Fig. 2 but for $a_L = 1$ and $\delta\ell = 5$. In bottom panel, in black the "+" solution of (26), while the green dashed curve is for the "−" solution. The left boundary of the figure corresponds to the kinematic cut-off $\ell_{\rm kin}$, or equivalently $p_\perp = 0$. (For interpretation of the references to color in this figure legend, the reader is referred to the web version of this article.)

curves which are displayed separately in the middle panels. (To some extent this mimics also a finite detector resolution.) Still the smoothed spectra exhibit a non-trivial gross structure with prominent peaks and some oscillatory sections.

We now turn to an interpretation of the gross structures. In doing so we employ the stationary phase (saddle point) approximation, cf. Eq. (25), which is based on $a_L/\eta \gg 1$; that is, the large frequency ratio ω_X/ω_L becomes here operationally to access also moderate laser intensities. According to the semi-classical interpretation *all* positrons are generated at $\ell = 0$ via the "bare" Breit–Wheeler process. The assisting laser field acting on these positrons shifts them in phase space due to the exchange of laser momentum and they end up at $\ell \neq 0$. Consequently, the spectrum of the positrons that is observed after the interaction with the laser is spread out essentially between the cut-off values $\ell_{\rm min} \leq \ell \leq \ell_{\rm max}$ (or equivalently $p_\perp^{\rm min} \leq p_\perp \leq p_\perp^{\rm max}$). Therefore, only for $\tau_X > \tau_L$ the "bare" Breit–Wheeler peak at $\ell = 0$ is clearly visible, when those positrons which are created before/after the laser impact remain at their place of birth in phase space. For smaller values of τ_X, the Breit–Wheeler peak vanishes since all positrons are shifted away upon the subsequent laser action. The cut-off values can be determined from the minimum and maximum values $\ell_\pm$ in Eq. (26). They read $\ell_{\rm max} = \ell^{(+)}$ and $\ell_{\rm min} = \min\left(\ell^{(-)}, \ell_{\rm kin}\right)$ with $\ell^{(\pm)} = s_{\rm thr} a_L/(\eta s_{X'X}) \left(a_L \pm 2\sqrt{s_{X'X}/s_{\rm thr} - 1}\right)$. The lower cut-off is influenced by the fact that the positron can lose at most its kinetic energy due to the laser action, it needs to retain at least its rest energy. That means $(1 + \eta\ell) s_{X'X} = M^2 \geq s_{\rm thr}$, yielding the kinematic cut-off $\ell > \ell_{\rm kin} = (s_{\rm thr}/s_{X'X} - 1)/\eta$. (The corresponding cut-off values for $p_\perp$ follow from Eq. (4).) Beyond the plateau region spanned by these cut-off values the spectra are going exponentially fast to zero.

The influence of the laser field intensity a_L is evident upon comparing Figs. 2 and 3: The minimum and maximum values of $p_\perp$, respectively ℓ, do strongly differ. A few, albeit not all, strong peaks can be attributed to spectral caustics in the spirit of [37]: These are the loci of merging branches of stationary phase points (see lower panels) determined by diverging $d\phi(\ell)/d\ell$ (see vertical lines in lower and upper panels). We use the notion of spectral caustics to denote the loci of accumulated and thus enhanced intensity in the spectrum of the generated positrons in momentum space, in analogy to optics where significant enhancement of light intensity occurs on a caustic in position space. The gray bands depict the estimated widths of the caustic zone by $\Delta\ell = (a_L/\eta)^{2/3}$, following from the universality of the caustic's properties [37,48].

The shape of the differential spectra in the region around the spectral caustics resembles indeed the caustics known from diffraction: They show the typical behavior of an Airy function describing the intensity distribution of light close to an optical caustic, e.g. that of the rainbow. This behavior is most pronounced at the upper cut-off values because only the caustic contributes there. For all the other peaks, the caustic contributions are accompanied by non-caustic contributions from the other branches of $\phi(\ell)$. This is particularly evident in Fig. 3. Moreover, the highly oscillatory behavior of the spectra can be explained as the interference from the contributions from the multiple stationary points.

The impact of the laser pulse length τ_L is obvious in comparing Figs. 3 and 4: The patterns of $\phi(\ell)$ are different (see lower panels) and, correspondingly, the spectra too (see upper panels). The shorter pulse implies fewer caustics with clearer correspondence to the prominent peaks in the transverse momentum spectra. At smaller values of a_L, the estimated widths of the caustics become too large and overlapping thus not supporting the caustical interpretation of the spectra. At larger values of a_L (e.g. $a_L \geq 3$) additional spectral modulation effects caused by the beating of the $\pm$ branches in (26) deserve separate investigations.

We would like to emphasize finally that the spectra exhibited in upper and middle panels of Figs. 2–4 depict the slice $z = 0$. There, the distributions are flat in z direction, i.e. gating experimentally on a $z \approx 0$ bin (corresponding to about 30 MeV positrons in the lab. frame for given parameters), e.g. by a Brown–Buechner spectrograph in the $\phi = \pi$ plane, is a prerequisite to have afterwards access to the $p_\perp$ spectra of interest. While leaving a discussion of a suitable experimental set-up for future work, we point out that the spectral caustic structures are not "washed out" by a superposition, e.g. of equally weighted spectra with 20% variation of a_L, thus enabling the access in multi-shot experiments. Besides observation

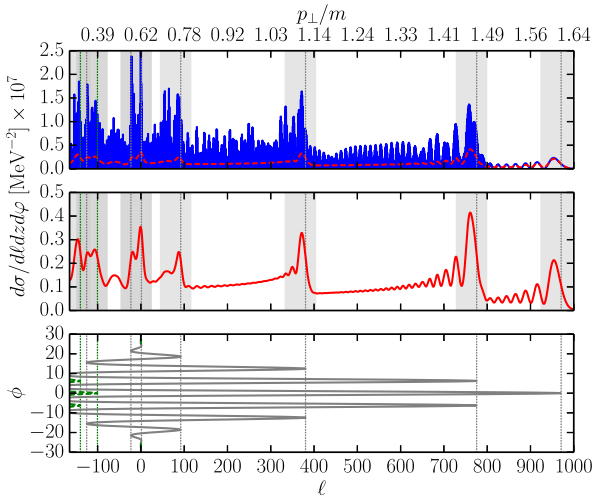

Fig. 4. As Fig. 3 but for the longer laser pulse duration $\tau = 8\pi$, resulting in a larger number of caustic peaks as compared to Fig. 3.

issues – which might be fairly challenging, in fact – we stress the relevance of the present investigation with respect to extensions of PIC codes aiming at simulating the formation of avalanches by seeded pair production (cf. [49]).

4. Summary

In summary we show that the differential spectra, most noticeably the transverse momentum distributions at fixed rapidity (more precisely, at $z = 0$ and fixed azimuthal angle of the positron) in laser assisted Breit–Wheeler pair production is strikingly modified by details of the lase pulse shape. One may attribute this phenomenon to a final state interaction of the once produced charged particles in the laser field. In other words, the quasi-classical motion with account of interference effects offers a key to the gross features of the spectra. On the one hand, the manifestation of the trajectories is not so surprising since the phase of the employed Volkov solutions for the $e^{\pm}$ wave functions encodes the classical Hamilton–Jacobi action. On the other hand, the convolution with other kinematic quantities of the squared matrix element is not so strong to destruct this trajectory information. The interpretation of the series of distinct peaks as spectral caustics, analog to laser assisted Compton scattering of X-rays, is semi-quantitative since obviously severe interference effects of the quantum mechanical propagation from certain phase points are, in general, responsible for the highly non-trivial final momentum distribution.

Finally, we speculate that the trident process, i.e. the seeded pair production in a virtual Compton process, may exhibit similar momentum signatures which could be also interpreted as spectral caustics. Corresponding experiments are possible with the set-ups planned by the HIBEF collaboration.

Acknowledgements

The authors acknowledge fruitful discussions with R. Sauerbrey and T.E. Cowan within the HIBEF project and A. Di Piazza, C.H. Keitel, H.R. Reiss, V.G. Serbo, R. Schützhold, G. Dunne, D. Blaschke, C. Müller, R. Alkofer, T. Heinzl, S. Fritzsche, and A. Surzhykov on elementary strong-field QED processes of contemporary interest.

References

[1] G. Breit, J.A. Wheeler, Phys. Rev. 46 (1934) 1087.
[2] A. Titov, B. Kämpfer, H. Takabe, Phys. Rev. Spec. Top., Accel. Beams 12 (2009) 111301.
[3] A. Titov, B. Kämpfer, H. Takabe, A. Hosaka, Phys. Rev. D 83 (2011) 053008.
[4] D. Burke, R. Field, G. Horton-Smith, T. Kotseroglou, J. Spencer, et al., Phys. Rev. Lett. 79 (1997) 1626.
[5] C. Bamber, S. Boege, T.K.T. Kotseroglou, A. Melissinos, et al., Phys. Rev. D 60 (1999) 092004.
[6] H. Hu, C. Müller, C.H. Keitel, Phys. Rev. Lett. 105 (2010) 080401.
[7] A. Di Piazza, C. Müller, K.Z. Hatsagortsyan, C.H. Keitel, Rev. Mod. Phys. 84 (2012) 1177.
[8] S. Meuren, C. Keitel, A. Di Piazza, arXiv:1503.03271, 2015.
[9] H.R. Reiss, J. Math. Phys. 3 (1962) 59.
[10] A.I. Nikishov, V.I. Ritus, J. Exp. Theor. Phys. 25 (1967) 1135.
[11] F. Sauter, Z. Phys. 69 (1931) 742.
[12] J. Schwinger, Phys. Rev. 82 (1951) 664.
[13] E. Brezin, C. Itzykson, Phys. Rev. D 2 (1970) 1191.
[14] V.S. Popov, Sov. J. Nucl. Phys. 19 (1974) 584.
[15] R. Schützhold, H. Gies, G. Dunne, Phys. Rev. Lett. 101 (2008) 130404.
[16] F. Hebenstreit, F. Fillion-Gourdeau, Phys. Lett. B 739 (2014) 189.
[17] A. Otto, D. Seipt, D. Blaschke, B. Kämpfer, S.A. Smolyansky, Phys. Lett. B 740 (2015) 335.
[18] L.S. Brown, T.W.B. Kibble, Phys. Rev. 133 (1964) A705.
[19] T. Nousch, D. Seipt, B. Kämpfer, A. Titov, Phys. Lett. B 715 (2012) 246.
[20] A. Titov, B. Kämpfer, A. Takabe, A. Hosaka, Phys. Rev. A 87 (2013) 042160.
[21] A. Titov, B. Kämpfer, A. Takabe, A. Hosaka, Phys. Rev. Lett. 108 (2012) 240406.
[22] M.J.A. Jansen, C. Müller, arXiv:1511.07660, 2015.
[23] K. Krajewska, J.Z. Kamiński, Phys. Rev. A 90 (2014) 052108.
[24] K. Krajewska, J.Z. Kamiński, Phys. Rev. A 86 (2012) 052104.
[25] C. Kohlfürst, H. Gies, R. Alkofer, Phys. Rev. Lett. 112 (2014) 050402.
[26] T. Heinzl, A. Ilderton, M. Marklund, Phys. Lett. B 692 (2010) 250.
[27] A. Ringwald, Phys. Lett. B 510 (2001) 107.
[28] http://www.xfel.eu/, 2015.
[29] http://www.hibef.eu, 2015.
[30] A. Jochmann, A. Irman, M. Bussmann, J.P. Couperus, T.E. Cowan, A.D. Debus, M. Kuntzsch, K.W.D. Ledingham, U. Lehnert, R. Sauerbrey, H.P. Schlenvoigt, D. Seipt, T. Stöhlker, D.B. Thorn, S. Trotsenko, A. Wagner, U. Schramm, Phys. Rev. Lett. 111 (2013) 114803.
[31] N.D. Powers, I. Ghebregziabher, G. Golovin, C. Liu, S. Chen, S. Banerjee, J. Zhang, D.P. Umstadter, Nat. Photonics 8 (2014) 28.
[32] W.P. Leemans, A.J. Gonsalves, H.-S. Mao, K. Nakamura, C. Benedetti, C.B. Schroeder, C. Tóth, J. Daniels, D.E. Mittelberger, S.S. Bulanov, J.-L. Vay, C.G.R. Geddes, E. Esarey, Phys. Rev. Lett. 113 (2014) 245002.
[33] S.G. Rykovanov, C.G.R. Geddes, J.-L. Vay, C.B. Schroeder, E. Esarey, W.P. Leemans, J. Phys. B 47 (2014) 234013.
[34] G. Sarri, D.J. Corvan, W. Schumaker, J.M. Cole, A. Di Piazza, H. Ahmed, C. Harvey, C.H. Keitel, K. Krushelnick, S.P.D. Mangles, Z. Najmudin, D. Symes, A.G.R. Thomas, M. Yeung, Z. Zhao, M. Zepf, Phys. Rev. Lett. 113 (2014) 224801.
[35] S. Corde, K. Ta Phuoc, G. Lambert, R.F.V. Malka, A. Rousse, A. Beck, E. Lefebvre, Rev. Mod. Phys. 85 (2013) 1.
[36] D. Seipt, B. Kämpfer, Phys. Rev. A 89 (2014) 023433.
[37] D. Seipt, S. Fritzsche, A. Surzhykov, B. Kämpfer, arXiv:1507.08868, 2015.
[38] M.J.A. Jansen, C. Müller, J. Phys. Conf. Ser. 594 (2015) 012051.
[39] A. Ilderton, G. Torgrimsson, J. Wårdh, Phys. Rev. D 92 (2015) 025009.
[40] A.A. Lebed', S.P. Roshchupkin, J. Exp. Theor. Phys. 113 (2011) 46.
[41] Y.-B. Wu, S.-S. Xue, Phys. Rev. D 90 (2014) 013009.
[42] S. Villalba-Chávez, C. Müller, Phys. Lett. B 718 (2013) 992.
[43] K.Z. Hatsagortsyan, A. Ipp, J. Evers, A. Di Piazza, C.H. Keitel, Proc. SPIE Int. Soc. Opt. Eng. 8080 (2011) 1T.
[44] I.V. Sokolov, N.M. Naumova, J.A. Nees, G.A. Mourou, Phys. Rev. Lett. 105 (2010) 195005.
[45] A. Di Piazza, Phys. Rev. D 70 (2004) 053013.
[46] L.D. Landau, E.M. Lifschitz, Course of theoretical physics, vol. 4, in: V.B. Berestetskii, E.M. Lifshitz, L.P. Pitaevskii (Eds.), Quantum Electrodynamics, Butterworth–Heinemann, 1982.
[47] A.I. Nikishov, V.I. Ritus, J. Exp. Theor. Phys. 19 (1964) 1191.
[48] Y.A. Kravtsov, Y.I. Orlov, Sov. Phys. Usp. 26 (1983) 1038.
[49] N.V. Elkina, A.M. Fedotov, I.Y. Kostyukov, M.V. Legkov, N.B. Narozhny, E.N. Nerush, H. Ruhl, Phys. Rev. Spec. Top., Accel. Beams 14 (2011) 054401.